Analysis and Optimization of Low-Pressure Drop Static Mixers

Mrityunjay K. Singh, Tae G. Kang, Patrick D. Anderson, and Han E. H. Meijer
Materials Technology, Eindhoven University of Technology, 5600 MB Eindhoven, The Netherlands

Andy N. Hrymak
Dept. of Chemical Engineering, McMaster University, Hamilton, ON L8S 4L7, Canada

DOI 10.1002/aic.11846
Published online July 6, 2009 in Wiley InterScience (www.interscience.wiley.com).

Various designs of the so called Low-Pressure Drop (LPD) static mixer are analyzed for their mixing performance using the mapping method. The two types of LPD designs, the RR and RL type, show essentially different mixing patterns. The RL design provides globally chaotic mixing, whereas the RR design always yields unmixed regions separated by KAM boundaries from mixed regions. The crossing angle between the elliptical plates of the LPD is the key design parameter to decide the performance of various designs. Four different crossing angles from 90° to 160° are used for both the RR and RL designs. Mixing performance is computed as a function of the energy to mix, reflected in overall pressure drop for all designs. Optimization using the flux-weighted intensity of segregation versus pressure drop proves the existence of the best mixer with an optimized crossing angle. The optimized angle proves to be indeed the LLPD design used in practice: the RL-120 with $\theta = 120°$*, although RL-140* $\theta = 140°$ *performs as good. Shear thinning shows minor effects on the mixing profiles, and the main optimization conclusions remain unaltered.* © 2009 American Institute of Chemical Engineers *AIChE J,* 55: 2208–2216, 2009

Keywords: chaotic mixing, bakers transformation, mapping method, static mixer, LPD mixer

Introduction

Homogenization of fluids is an essential and elementary step in many processes of industrial operations. Examples include food processing, paint making, numerous chemical processes, pharmaceutical fabrication, polymer processing, etc. Turbulence is frequently applied to obtain good mixing in industrial processes, but in case of mixing of high-viscosity fluids, as in food and polymer processing, turbulence is not achievable. Well-designed laminar flow can, however, produce irregular trajectories of fluid particles, resulting in efficient mixing via chaotic advection.[1,2] This can be achieved in both dynamic and static mixers. A large number of continuous static mixers have been designed on this principle, the Kenics,[3] Ross interfacial surface generator (ISG) and Ross low-pressure drop (LPD),[4] the Sulzer SMX,[5] and the multiflux mixer.[6] All these mixer designs are based on the principle that mimics the bakers transformation: a continuous repetition of stretching, cutting, and stacking.

From all static mixers, the Kenics mixer has been analyzed most,[7,12] followed by the Sulzer SMX.[13–15] Only a few studies are reported on LPD mixers, see e.g. Rauline[16] and, in this study, we therefore analyze and optimize the LPD geometry. Apart from studying Newtonian fluids, also the effect of shear thinning is taken into account. The mapping method is used in this analysis, as it provides a distribution matrix and allows to compute the redistribution of material during any specified flow. In spatially or time

Correspondence concerning this article should be addressed to P. D. Anderson at p.d.anderson@tue.nl

periodic flows, the mapping matrix is computed only once for one period. In a subsequent postprocessing operation, concentration distributions for all following periods are computed using a vector (mapping) matrix-(concentration) multiplication, which is computationally very fast. The method allows us to compute quantitative mixing measures, like the intensity of segregation and scale of segregation, that provide an objective function to compare various mixing designs. In this study of the LPD static mixers, we will use the cross-sectional area averaged flux-weighted intensity of segregation as the measure of mixing and the pressure drop, needed to arrive at a desired mixing quality, as the energy input needed. Optimization is defined as finding the lowest value of the intensity of segregation for the lowest pressure drop required. Here, the length of the mixer is not used as a criterion.

The article is organized as follows. First, we start with introducing the different LPD designs and the problem at hand, followed by describing the typical characteristics of the flow fields inside the LPD mixers. Second, we describe the method used to analyze mixing where we briefly introduce the mapping method. Finally, we summarize the most relevant outcomes of the mixing analyses and optimization results and draw conclusions.

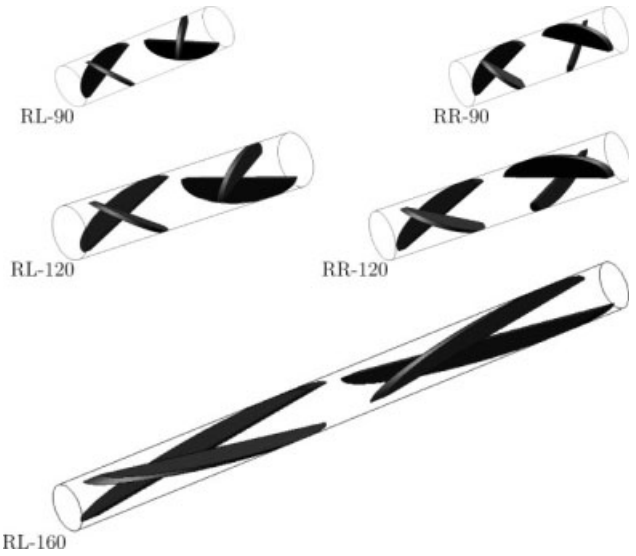

Figure 1. Various LPD designs with different crossing angle: RL and RR layouts of mixer.

Geometries and flow fields

Figure 1 shows a number of different designs of the LPD mixer with varying configuration and crossing angle illustrating the two types of designs of the LPD. We will use the notation RL and RR as previously done for the two similar types of Kenics designs.[9–12] The LPD consists of a series of semielliptical plates positioned in a tubular housing. Two neighboring plates form an element and two elements form the basic periodic unit of the LPD. The first element in both the RL-90 and the RR-90 design consists of two opposite plates crossing at angle of 90° with respect to each other. In the RR design, the second element is an identical copy of the first element rotated by 90° in tangential direction, whereas in the RL design the rotation is accompanied by mirroring. The crossing angle between the two semielliptical plates, gives specific layouts, see Figure 1 for some examples like: RL-90, RL-120, RL-140, and RL-160 with crossing angles of 90°, 120°, 140°, and 160°, respectively. An increase in the crossing angle implies an increase in the axial length of the design. The RL-120 design is also known as the low–low–pressure drop (LLPD) mixer.[4] As fluid flows through the device, the crossing angle determines the amount of stretching per element, before re-orientation of the flow on entering the perpendicular second element. Hence, the question arises what is the optimum crossing angle to achieve the best mixing at a minimum pressure drop. This optimization study will be performed here for both Newtonian and non-Newtonian fluids, because different velocity fields result which can influence the mixing performance.

We perform full three-dimensional computations of velocity field in all the designs of the LPD. The geometries used are: radius $R = 1.332$ cm, axial gap between two neighboring elements $l_g = 0.5$ cm, thickness of blades $t = 0.2$ cm, and the length of the one periodic unit of RL-90, RL-120, RL-140, and RL-160 are 6.9, 11.0, 16.8, and 33.5 cm, respectively. The RR counterparts of course have the same length as the RL designs. Unstructured tetrahedral mesh is obtained with Gambit V2.1.2 for each design of the mixer, and Fluent V6.1.22 is used to get the 3D velocity field. The mesh size for the smallest design, the RL-90, consists of 948053 cells with 174152 nodes, whereas the mesh for longest design, the RL-160, consists of 1794412 cells with 341340 nodes. The average time to get converged velocity field is around 8 CPU hours on a PC with AMD Athlon processor, 2.4 GHz, 1 GB RAM. In the Newtonian case, a fluid with density $\rho = 846$ kg/m^3, and viscosity $\mu = 1$ kg m/s is considered. To study the effect of shear thinning on mixing, the Carreau model is used to describe the non-Newtonian viscosity μ of the fluid:

$$\mu = \mu_\infty + (\mu_0 - \mu_\infty)[1 + \lambda^2 |II_{2D}|]^{\frac{n-1}{2}}, \tag{1}$$

where μ_0 is the viscosity at zero shear rate, and II_{2D} is the second invariant of the rate of deformation tensor. The time contant parameter λ is fixed at $\lambda = 10$, which ensures that the shear thinning region is achieved in the LPD designs. Two values of the power coefficient $n = 0.4$ and 0.8 are considered. For the velocity field computations, periodic boundary conditions are prescribed between inlet and outlet, and at the inlet a mass flow rate $\dot{m} = 4.714 \times 10^{-3}$ kg/s is imposed. The Reynolds number, Re ($= \rho\, u\, D/\mu$, where D is the diameter), is below 10^{-2} for all simulations. Hence, the flow is clearly in the Stokes regime. Note that mixing simulations based on these velocity fields are valid for any material properties in Stokes flow regime.

The differences in second element of RL and RR of a periodic LPD design lead to different characteristic of transverse velocity during one flow period. Figure 2 shows the transverse velocity vectors plotted for RL and RR designs at two positions: in the middle of the first and second element, respectively. The RL design produces two counter-clockwise flows followed by two clockwise flows, whereas the RR design induces two counter-clockwise flows followed by two counter-clockwise flows. Two successive

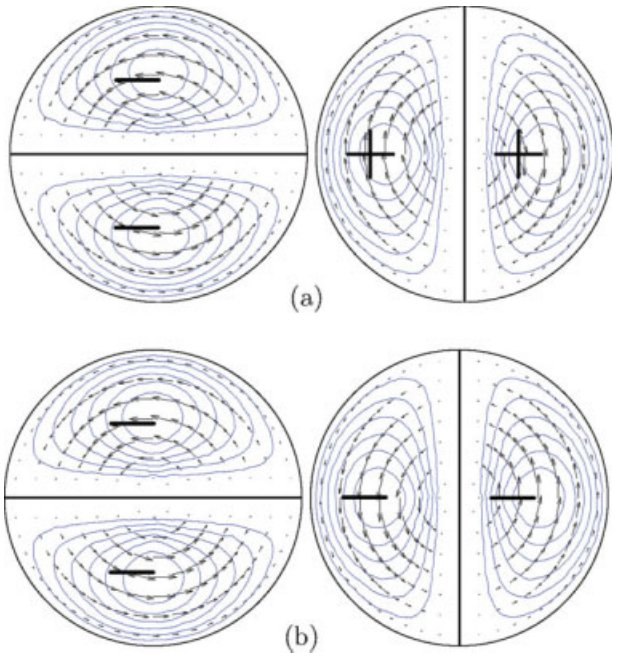

Figure 2. Cross-sectional flows in the middle of the first (left) and second (right) element for the LPD-90 mixers: (a) RL and (b) RR design.

The "+" and "−" indicate the clockwise and counterclockwise motion. [Color figure can be viewed in the online issue, which is available at www.interscience.wiley.com.]

elements of both mixers show intersecting streamlines, when projected onto the same plane (x,y), which is the key to achieve chaotic mixing. According to the linked twist map (LTM) theorem[17–19] the counter-rotating (alternating clockwise and counterclockwise) layouts (e.g., the RL design of LPD) provide better mixing when compared with corotating layouts (e.g., the RR design of LPD). This has already been shown in the Kenics mixer, where RL designs of the Kenics always provide much better mixing than RR designs. The same conclusion was drawn in a recently developed mixing device known as RAM,[20–23] where it has been demonstrated that the counter-rotating designs are candidates for producing globally chaotic mixing, whereas corotating designs lack this capability. Still, the question remains which RL design is the best, and in addition, how worse is the performance of the RR designs with respect to the RL designs.

Methods and Measures

Mapping method

The mapping method has proven to be a powerful method to analyze and optimize distributive mixing in various mixers and protocols.[8,9,24–27] The original approach of mapping uses interfacial tracking of discretized cells to find the mapping coefficients. However, it is cumbersome to track interfaces experiencing complicated deformation patterns and in some cases it is almost impossible to track interfaces. Recently, we formulated an alternative approach to find the mapping coefficients that is much simpler to implement.[23,28,29]

Figure 3 depicts how the mapping coefficients are computed in the new formulation of the method. To approximate the coefficients of the mapping matrix (or distribution matrix), K markers inside all cells are tracked. The markers are uniformly distributed in the cells. Then, to determine the final distribution of markers, they are advected during the flow from $z = z_0$ to $z = z_0 + \Delta z$. If the number of markers in the donor cell Ω_j is M_j at $z = z_0$ and the number of markers found after tracking in the recipient cell Ω_i is M_{ij} at $z = z_0 + \Delta z$, then the mapping coefficient Φ_{ij} is calculated as:

$$\Phi_{ij} = \frac{M_{ij}}{M_j}. \tag{2}$$

In other words, the coefficient Φ_{ij} is the measure of the fraction of the total flux of cell Ω_j donated to cell Ω_i.

The elegance of the mapping method is that if one wants to analyze mixing-related quantities, like the concentration vector $\boldsymbol{C} \in \mathbb{R}^{N\times 1}$ (N is the number of cells) defined on initial cells, then the concentration evolution $\boldsymbol{C}^1$ after the deformation can be obtained by simply multiplying the mapping matrix Φ with the initial concentration vector $\boldsymbol{C}^\circ$:

$$\boldsymbol{C}^1 = \Phi \boldsymbol{C}^\circ. \tag{3}$$

Note that $\boldsymbol{C}$ represents the coarse-grained description of volume fraction (dimensionless concentration) of a marker fluid in a mixture of two marker fluids with identical material properties, and its component C_i describes the concentration (volume fraction) locally averaged in the cell Ω_i. For repetitive mixing, the same operation is repeated multiple times on the same mass and, hence, the concentration evolution after n steps is given by $\boldsymbol{C}^n = \Phi^n \boldsymbol{C}^\circ$. For sufficiently large n, the matrix Φ^n will not be sparse and it becomes that large that it can even not be stored anymore. This is due to the fact that after performing the operation n times, material from one cell is advected to a large part of the whole cross-section, especially in the case of chaotic advection. Instead of studying Φ^n, the evolution of the concentration after n steps $\boldsymbol{C}^n$ is computed in sequence as follows:

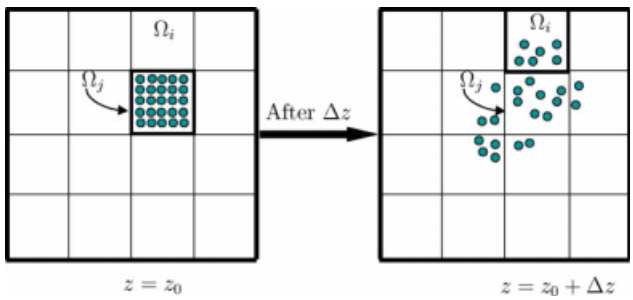

Figure 3. Illustration of the computation of the coefficients Φ_{ij} of the mapping matrix Φ.

The cell Ω_j at $z = z_0$ is covered with a number of markers that are tracked during flow in Δz (to arrive at the final cross section $z = z_0 + \Delta z$). The ratio of the number of markers received by the recipient cell Ω_i to the initial number of markers in Ω_j is determined (in this example Φ_{ij} is $\frac{6}{25}$). [Color figure can be viewed in the online issue, which is available at www.interscience.wiley.com.]

$$\boldsymbol{C}^{i+1} = \Phi \boldsymbol{C}^{i}, \text{ hence } \boldsymbol{C}^{n} = (\underbrace{\Phi(\Phi(\ldots(\Phi}_{n \text{ times}} \boldsymbol{C}^{\circ})))). \quad (4)$$

Thus, the mapping matrix Φ is determined only once and is used a number of times to study the evolution of concentration in the flow field. Computation of mapping matrices is expensive, and may take several CPU hours, but, once calculated, the necessary matrix-vector multiplication only takes a few CPU seconds to process the results. The mapping matrix calculations are easily parallelized.[25]

Measure of mixing

To compare various layouts of the LPD mixer, we use the flux-weighted discrete intensity of segregation defined in a cross-section, using the coarse grain concentration C_i in the mapping cells as a mixing measure (see Singh et al.[28] for details):

$$I_{\mathrm{d}} = \frac{1}{\bar{C}(1-\bar{C})} \frac{1}{F} \sum_{i=1}^{N} (C_i - \bar{C})^2 f_i, \quad (5)$$

where the average concentration $\bar{C}$ is

$$\bar{C} = \frac{1}{F} \sum_{i=1}^{N} C_i f_i, F = \sum_{i=1}^{N} f_i. \quad (6)$$

The term f_i is the volumetric flux through cell number i, F is the total flux through the mixer, and N is the number of total cells in the domain. The intensity of segregation I_{d} is a measure of the deviation of the local concentration from the ideal situation (perfectly mixed case), which represents a homogeneous state of the mixture. In a perfectly mixed system, $I_{\mathrm{d}} = 0$, whereas in a completely segregated system, $I_{\mathrm{d}} = 1$. As found by Galaktionov et al.,[8,9] the flux-weighted definition (see Eq. 5) of the intensity of segregation is much better suited for analyzing continuous mixers than area- or volume-averaged definitions of the intensity of segregation. This is due to the fact that the real impact of an unmixed island (or chaotic region) in the flow on the quality of mixing is proportional to the flux, carrying this island (or chaotic region).

Defining the mapping matrices of the LPD

For the calculation of a mapping matrix, the cross-sectional area is divided into 200 $\times$200 grids, and the number of particles per cell (NPPC) used is 100 (10$\times$10 array of particles). Note that the NPPC should be sufficient so that a converged mixing measure $\mathrm{I_d}$ is obtained.[28] The position of the particles are tracked by solving the following set of equations:

$$\frac{\mathrm{dx}}{\mathrm{dz}} = \frac{u_x}{u_z}, \frac{\mathrm{dy}}{\mathrm{dz}} = \frac{u_y}{u_z}, \quad (7)$$

where u_x, u_y, and u_z are x, y, and z (axial) components of the velocity vector. In this approach, integration is done with respect to the down-channel direction z, which is appropriate to determine the planar locations of the particles after one period. This approach is only valid for the systems where the down-channel velocity components are always positive, if this is not the case, time integration must be performed.[23] To solve Eq. 7, we use the fourth-order Runge–Kutta Bulrish Store scheme with the adaptive step size selection.[30]

To do a full analysis of mixing of each LPD design, we compute two separate mapping matrices Φ_i (i = 1, 2) representative for each element of the LPD design. Later, these matrices are used to study the concentration evolution in a sequence (Eq. 4).

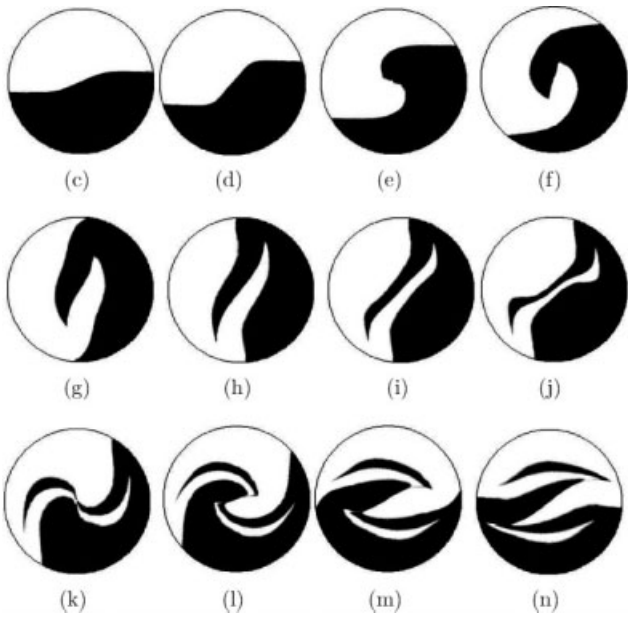

Figure 4. Working principle of RL design of the LPD: Mixing profiles after each $\frac{1}{6}$L of the element.

Here, L is the length of one blade.

Results

Working principle of the standard LPD mixer

To illustrate the working principle of the RL design of the LPD static mixer, a series of concentration profiles at locations of each $\frac{1}{6}L$ where L is the length of one element, is shown in Figure 4 for a standard LPD with 90° crossing angle. Figures 4a–f shows the concentration evolution along the first element, whereas Figures 4g–l shows the subsequent profiles in the second element. For these computations, we used a LPD design with a zero blade thickness to understand the basic mixing mechanisms. All 12 mapping matrices Φ_i (i = 1, 2, 3, …, 12) are computed to get the exact concentration profiles $\boldsymbol{C}^i$. We easily recognize the interface stretching caused by the rotation imparted by the transverse flow in the first element (see Figures 4a–f). As the interface enters the second element (see Figures 4g), the start of perpendicular folding occurs followed by subsequent stretching (see Figures 4h–l). Figure 4i shows the mixing pattern just at middle of the second element illustrating how the striations created are folded and being relocated in the cross-section. As a result of the folding and stretching actions, the number of striations is doubled at the end of second element (see Figures 4l). Compared with the ideal bakers transformation, that indeed can be realized in practice, e.g., with the multiflux mixer, as shown in Figure 5,[31] the layers created are not of the same thickness

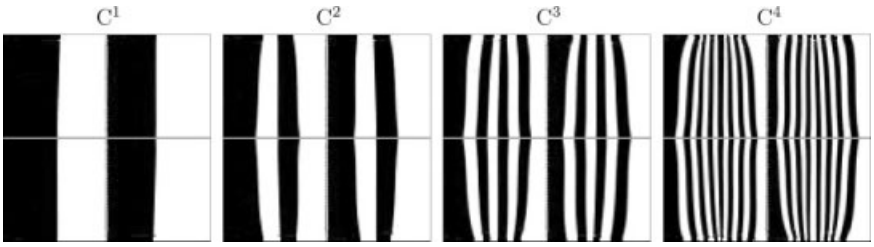

Figure 5. Demonstration of bakers transformation in a multiflux static mixer: Mixing profiles C^1, C^2, C^3, and C^4 are concentration distributions after 1, 2, 3, and 4 periods of mixing.

With each element 2^n interfaces covering whole the cross-section with almost equal thickness of layers are generated.[31]

and do not cover the total cross-sectional length. This demonstrates that a larger crossing angle is required to provide interfaces created with a larger length. Hence, this indicates that there is still room for improvement.

Figure 6 shows the mixing patterns for the RR design on exactly the same positions as shown for the RL design in Figure 4. As, the first element of both designs are identical, Figures 4a–f and 6a–f are identical. Even Figures 4f and 6f are the same, thus the difference in the transition region between the first and the second element in the RL and RR design apparently does not influence the upstream flow. However, a clear difference in profiles starts to be visible once the fluid enters the second element (cf. Figures 4g and 6g). The most noticeable difference is that the RR design always rotates the interface in counter-clockwise direction, whereas in RL designs both counter-clockwise and clockwise movement of interface is realized (even more clear by comparing Figures 7 and 8 of the next section). This is due to the difference in direction of the transverse velocity present in the second element of the both designs (see Figure 2): the RR design always yields counter-clockwise transverse velocities, whereas the RL design provides both counter-clockwise as well as clockwise transverse velocities. The movement of interface monotonically in same direction in RR designs hinders mixing of some parts of the black material with the white material leading to two unmixed islands, whereas opposite movement of interface after each element in RL designs allows to mix all parts well leading to chaotic mixing (this is evident by comparing Figures 7 and 8 of the next section).

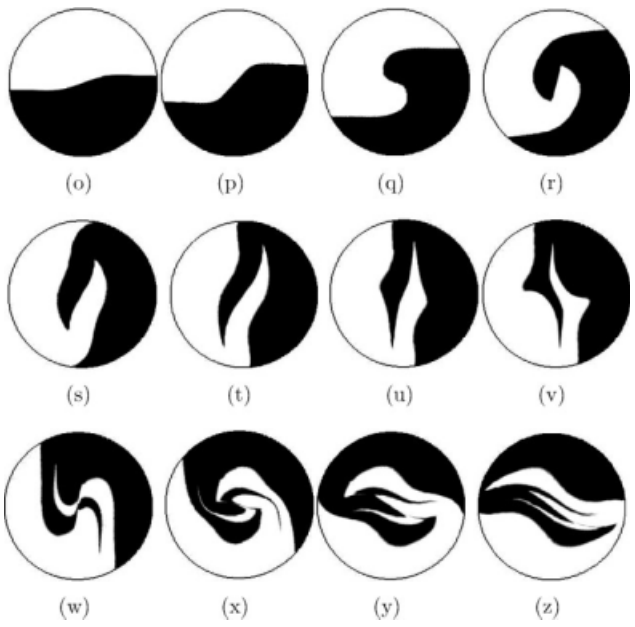

Figure 6. Working principle of RR design of LPD: Mixing profiles after each $\frac{1}{6}L$ of the element.

Here, L is the length of one blade.

Optimization of the LPD mixer

Optimization of the LPD mixer concerns the finding of the optimum crossing angle between the two elements that

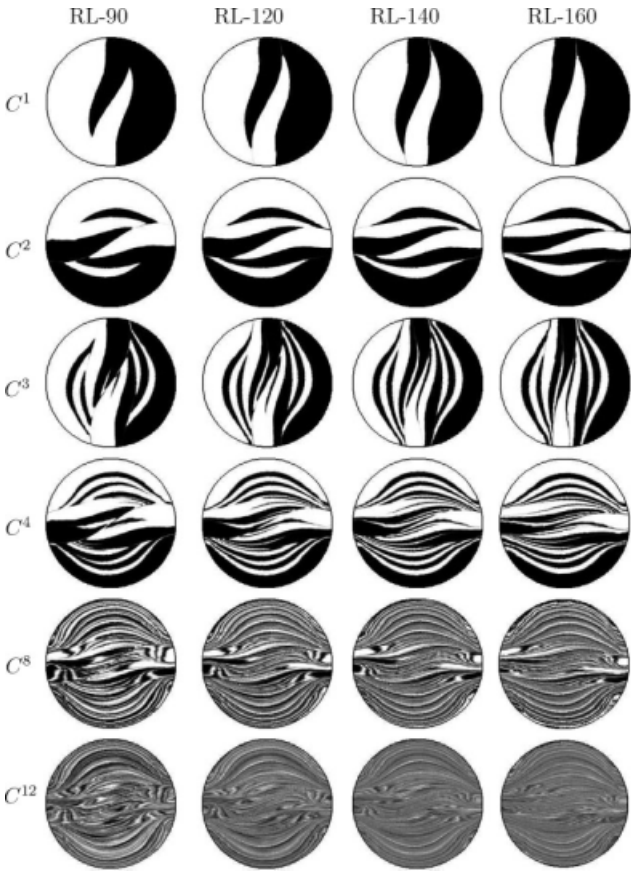

Figure 7. Mixing profiles for various RL designs of LPD mixer.

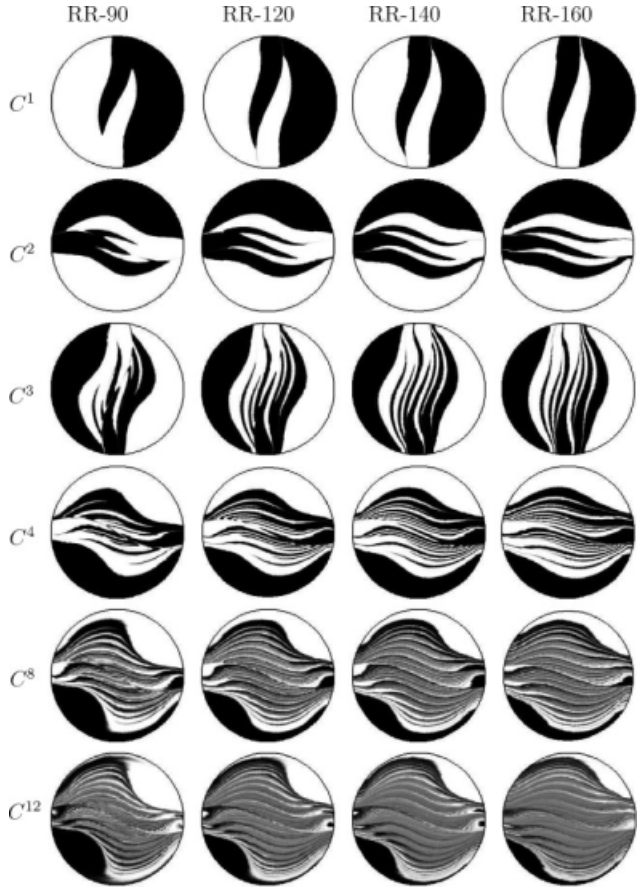

Figure 8. Mixing profiles for various RR designs of LPD mixer.

comprise the mixer such that the best mixing is achieved using a minimum pressure drop. Four crossing angles are considered 90°, 120°, 140°, and 160°. Note that any change in crossing angle necessitates to compute a new velocity field. As described in sub-section Defining the mapping matrices of the LPD, two mapping matrices Φ_i ($i = 1, 2$) are computed corresponding to the two elements of a specific design of the LPD and then the concentration distribution is obtained in the sequence using Eq. 4. Figure 7 shows the mixing profiles for RL design of the LPD after 1, 2, … , 4, 8, and 12 elements. All mixers seem to work well, but inspection reveals that on increasing the crossing angle from 90° to 160°, the striations are stretched further in each elementary mixing step and cover more of the cross-sectional length. The mixing profile after the first element, C^1 reveals that in the RL-90 design, the striations cover almost three fourth of the cross-sectional length, whereas the RL-120 design shows stretching over a larger part of the cross-section. Comparing with that, the changes in striation distributions for the RL-140 to RL-160 designs are still improving, but of course at costs of length and pressure drop per unit. From the qualitative mixing profiles, it is evident that the RL-160 is the best design to achieve the fastest mixing per element, but this does not mean that the design is most efficient regarding the overall pressure drop. Interestingly, increasing the crossing angle decreases the axial pressure gradient (also reflected in the nomenclature used: LPD for RL-90 design and LLPD for the RL-120 design), but increases the length of the elements and therefore, after a critical crossing angle, an increase in total pressure drop per period is the result. Therefore, we should compare both the total pressure drop and mixing capability of a design. To judge this, the flux-weighted intensity of segregation I_d is plotted as a function of the pressure drop, see Figure 10a. Clearly, an optimum crossing angle exists. The RL-120 and RL-140 designs have almost comparable performance and indeed, the weaker performance of the standard RL-90 design, as well as the extreme RL-160 design, in terms of pressure drop (read energy consumption required to achieve good mixing) is evident. On the other hand, the absolute axial length of a periodic unit of RL-140 design is significantly larger than that of the RL-120 design. On the basis of the pressure drop requirements and length restrictions, we can conclude that the optimum design is RL-120.

Figure 8 shows the mixing profiles for the RR design of the LPD mixer after 1, 2, … , 4, 8, and 12 elements. Interestingly, where the RL design of the LPD resembles the results of the RL-180 Kenics design, compare Figures 7 and 9 (top), the concentration profiles of the RR design show similar mixing patterns as obtained in RR-180 Kenics mixer design, compare Figures 8 and 9 (bottom). Irrespective of the crossing angle, all the RR designs always exhibit KAM (Koglomorov–Arnold–Moser) boundaries separating unmixed regions in the total domain from the well mixed regions. Because of the presence of these isolated unmixed regions, the RR designs are bad mixing designs, and increasing the crossing angle only reduces the size of the unmixed islands instead of resulting in a complete removal from the total

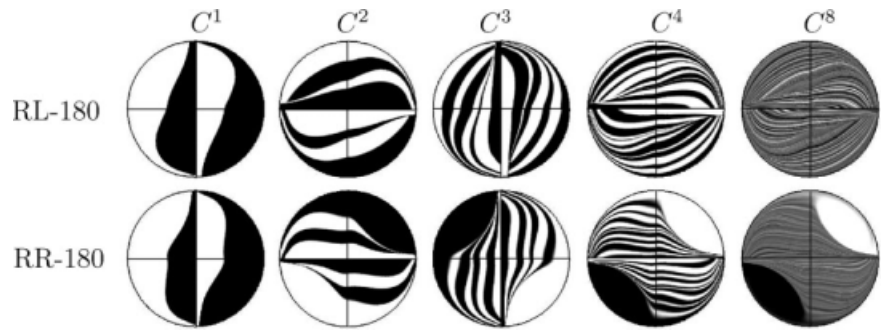

Figure 9. Mixing profiles for RL-180 and RR-180 design of Kenics mixer.[9]

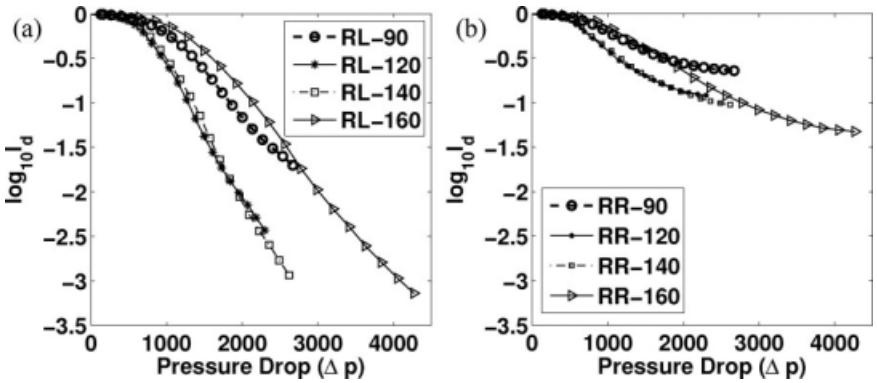

Figure 10. Comparing mixing performance of LPD designs: (a) RL design and (b) RR design.

The unit of pressure drop used here is N/m^2.

cross-section. From plotting the flux-weighted intensity of segregation versus pressure drop for the RR designs, see Figure 10b, we conclude that the RL design is almost 10 times more efficient than their counterpart RR designs.

Effect of shear thinning

As mentioned in Section Geometries and Flow Fields, the Carreau model with power law index $n = 0.4$ and 0.8 is used to study the effect of shear thinning on mixing. Figure 11 compares qualitative mixing profiles for the RL-120 design for Newtonian and non-Newtonian cases. Clearly, only minor differences in mixing patterns are detected. To compare mixing quantitatively, the flux-weighted intensity of segregation is plotted as a function of the pressure drop for the RL-120 design, as shown in Figure 12a. It is clear from this plot that shear thinning causes lower pressure drops for the same mixing quality and for $n = 0.4$ pressure consumption is lower than $n = 0.8$, which on its turn is better than Newtonian $n = 1$. However, this judgment of mixing efficiency is unfair, because this increase in efficiency is only due to a large reduction in viscosity eventually leading to a far lower pressure drop per period for the non-Newtonian cases. To overcome this problem, we calculate a scaling factor for the pressure drop on the basis of the viscosity at an apparent shear rate using Eq. 1. We assumed here an apparent shear rate of five times that of an empty tube (note that for SMX static mixer, an apparent shear rate of around seven times that of an empty tube is found[32]) and the apparent shear rate in an empty tube equals $\frac{8\langle u\rangle}{D}$, where $\langle u\rangle$ is the average inlet velocity and D is the diameter. Substituting the value of apparent shear rate in Eq. 1 provides a scaling factor ($p^* = p \times \frac{\mu_0}{\mu}$) close to 2.7 for $n = 0.8$ and 20.2 for $n = 0.4$. Figure 12 shows the plot of intensity of segregation as a function of scaled pressure drop p^*, now revealing that $n = 0.8$ provides better mixing when compared with the Newtonian case, whereas $n = 0.4$ provides somewhat worse mixing when compared with the Newtonian case. This result confirms that comparing mixing quality based on pressure drops makes less sense for shear thinning fluids. To overcome these ambiguities, we plot the flux weighted intensity of segregation as a function of length of the mixer as shown in Figure 13 for RL-90 and RL-120 designs.This can also be thought as providing the same pressure drop as for the Newtonian case to force the fluid through the devices, irrespective of the power law index n. The change in mixing quality

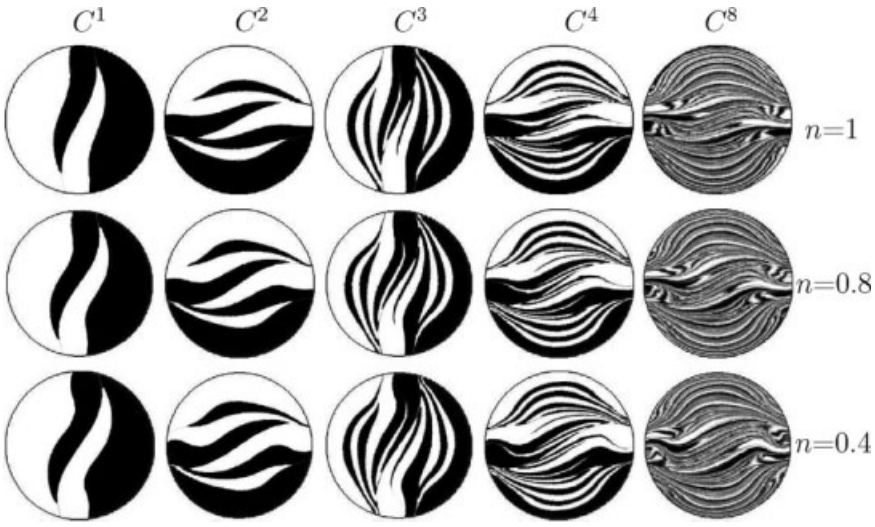

Figure 11. Effect of shear thinning on mixing profiles for RL-120 design.

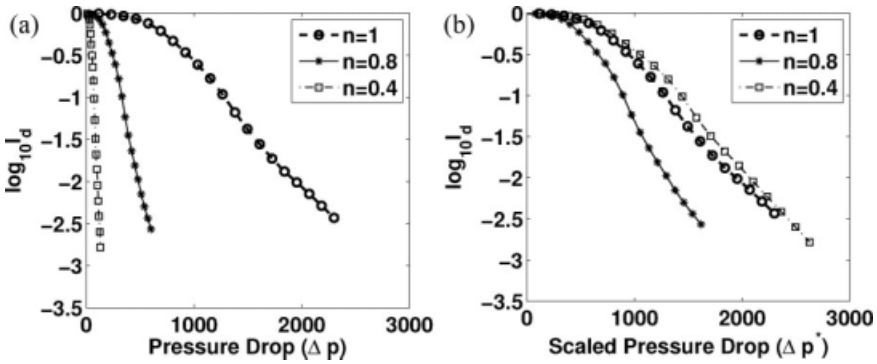

Figure 12. Quantifying mixing performance of LPD designs for shear thinning fluids for RL-120 design: (a) Intensity of segregation I_d versus pressure drop and (b) I_d versus scaled pressure drop p^* ($p^* = p \times \frac{\mu_0}{\mu}$).

The unit of pressure drop used here is N/m^2.

with length reveals almost negligible dependence on fluid rheology (see Figure 13b in complete accordance with the qualitative patterns in Figure 11), but for the shear thinning fluids the flux can be much higher for the same overall pressure drop. A point of caution is that the velocities imparted at inlet should not cross the limit of the Stokes regime in this way. Also for other designs, the previous conclusions are found to be true, and overall this leads to the conclusion, the optimum design is still the LLPD RL-120.

Conclusions

Mixing in LPD static mixers is analyzed using the mapping method. The two types of designs of the LPD mixer, RL and RR, show different characteristic velocities during one flow period, characterized as alternating counter and corotating for the RL design versus continuously counter-rotating for the RR design. This influences the way stretched interfaces are folded when fluid passes from one element to the next, and greatly determines the efficiency of mixing. Apart from the successive directions of rotation, the crossing angle between two blades of a single element of the LPD mixer is the most important design parameter to decide the quality of mixing. As the crossing angle increases, stretching of interfaces formed is more closer to those in an ideal bakers transformation occupying the complete cross-sectional length D, the diameter of the mixer. Although with increasing crossing angle, the axial pressure gradient decreases, the length of a periodic unit increases and, therefore, after a certain crossing angle the pressure drop per period starts to increase. Hence, overall a tradeoff between pressure drop and the mixing via improved stretching is required to optimize the designs. Applying the mapping method, we find that mixing profiles for the RL and RR design show quite drastic differences, KAM boundaries are detected in the RR design irrespective of the choice of the crossing angle, whereas the RL design is able to provide globally chaotic mixing. Comparing the performance of various designs with different crossing angle proves that the RL-120 design is the optimum and that the RL-140 performs as good but needs a larger axial length for this performance. The RL designs are almost 10 times more efficient than their counterpart RR designs, because of the presence of KAM boundaries in the later designs. Shear thinning effects show minor influence on mixing in these LPD static mixers.

Acknowledgement

This work was supported by Dutch Polymer Institute (DPI) (grant # 446).

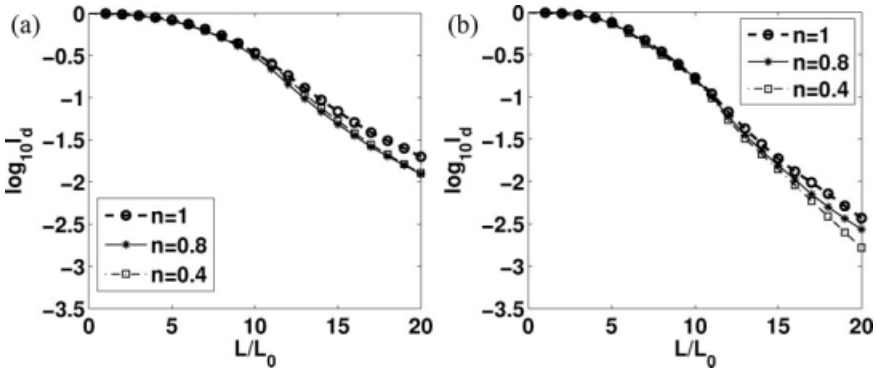

Figure 13. Quantifying mixing performance of LPD designs for shear thinning fluids using I_d versus length: (a) RL-90 and (b) RL-120.

Here, L_0 is length of periodic unit of the respective design.

Literature Cited

1. Aref H. Stirring by chaotic advection. *J Fluid Mech*. 1984;143:1–21.
2. Ottino JM. *The Kinematics of Mixing: Stretching, Chaos, and Transport*. Cambridge: Cambridge University Press, 1989.
3. Chemineer-web. Available at: www.chemineer.com. 2008
4. Ross-web. Available at: www.staticmixers.com. 2008.
5. Sulzer-web. Available at: www.sulzerchemtech.com. 2008.
6. Sluijters R. Het principe van de multiflux menger. De Ingenieur. *Chemische Techniek 3*. 1965;77:33–36.
7. Byrde O, Sawley ML. Parallel computation and analysis of the flow in a static mixer. *Compute and Fluids*. 1999;28:1–18.
8. Galaktionov OS, Anderson PD, Peters GWM, Meijer HEH. Morphology development in Kenics static mixers (Application of the extended mapping method). *Can J Chem Eng*. 2002;80:604–618.
9. Galaktionov OS, Anderson PD, Peters GWM, Meijer HEH. Analysis and optimization of Kenics mixers. *Int Polym Proc*. 2003;18:138–150.
10. Hobbs DM, Muzzio FJ. The Kenics static mixer: a three-dimensional chaotic flow. *Chem Eng J*. 1997;67:153–166.
11. Hobbs DM, Swanson PD, Muzzio FJ. Numerical characterization of low Reynolds number flow in the Kenics static mixer. *Chem Eng Sci*. 1998;53:1565–1584.
12. Hobbs DM, Muzzio FJ. Reynolds number effects on laminar mixing in the Kenics static mixer. *Chem Eng J*. 1998;70:1942–1952.
13. Zalc JM, Szalai ES, Muzzio FE, Jaffer S. Characterization of flow and mixing in an SMX static mixer. *AIChE J*. 2002;48:427–436.
14. Mickaily-Hubber ES, Bertrand F, Tanguy P, Meyer T, Renken A, Rys FS, Wehrli M. Numerical simulations of mixing in an SMRX static mixer. *Chem Eng J*. 1996;63:117–126.
15. Liu S, Hrymak AN, Wood PE. Laminar mixing of shear thinnning fluids in a SMX static mixer. *AIChE J*. 2006;52:152–157.
16. Rauline D, Tanguy PA, Blévec JML, Bousquet J. Numerical investigation of the performance of several static mixers. *Can J Chem Eng*. 1998;76:527–535.
17. Wiggins S, Ottino JM. Foundations of chaotic mixing. *Phil Trans R Soc London A*. 2004;362:937–970.
18. Ottino JM, Wiggins S. Designing optimal micromixers. *Science*. 2004;305:485–486.
19. Sturman R, Ottino JM, Wiggins S. *The Mathematical Foundations of Mixing the Linked Twist Map as a Paradigm in Applications: Micro to Macro, Fluids to Solids*. Cambridge: Cambridge University Press, 2006.
20. Metcalfe G, Rudman M, Brydon A, Graham L, Hamilton R. Composing chaos: An experimental and computational study of an open duct mixing flow. *AIChE J*. 2006;52:9–28.
21. Speetjens M, Rudman M, Metcalfe G. Flow regime analysis of non-Newtonian duct flows. *Phys Fluids*. 2006;18:013101, DOI: 10.1063/1.2163913.
22. Speetjens M, Metcalfe G, Rudman M. Topological mixing study of non-Newtonian duct flows. *Phys Fluids*. 2006;18:103103, DOI: 10.1063/1.2359698.
23. Singh MK, Anderson PD, Speetjens MFM, Meijer HEH. Optimizing the rotated arc mixer. *AIChE J*. 2008;54:2809–2822.
24. Anderson PD, Meijer HEH. Chaotic mixing analyses by distribution matrices. *Appl Rheol*. 2000;10:119–133.
25. Galaktionov AS, Anderson PD, Peters GWM. Mixing simulations: tracking strongly deforming fluid volumes in 3D flows, In: Bubak JDM, Wasniewski J, editors. *Lecture Notes in Computer Science, volume 1332 of Recent advances in Parallel Virtual Machine and Message Passing Interface*. Springer, 1997; 463–469.
26. Kruijt PGM, Galaktionov OS, Anderson PD, Peters GWM, Meijer HEH. Analyzing mixing in periodic flows by distribution matrices: mapping method. *AIChE J*. 2001;47:1005–1015.
27. Kruijt PGM, Galaktionov OS, Peters GWM, Meijer HEH. The mapping method for mixing optimization. II. Transport in a corotating twin screw extruder. *Int Polym Proc*. 2001;16:161–171.
28. Singh MK, Kang TG, Meijer HEH, Anderson PD. The mapping method as a toolbox to analyze, design and optimize micromixers. *Microfluidics Nanofluidics*. 2008;5:313–325.
29. Kang TG, Singh MK, Kwon TH, Anderson PD. Chaotic mixing using periodic and aperiodic sequences of mixing protocols in a micromixer. *Microfluidics Nanofluidics*. 2008;4:589–599.
30. Press WH, Teukolsky SA, Vetterling WT, Flannery BP. *Numerical Recipes in FORTRAN*. New York: Cambridge University Press, 1992.
31. Van der Hoeven JC, Wimberger-Friedl R, Meijer HEH. Homogeneity of multilayers produced with a static mixer. *Pol Eng and Sci*. 2001;41:32–42.
32. Liu S, Hrymak AN, Wood PE. Design modifications to SMX static mixer for improving mixing. *Chem Eng Sci*. 2006;61:1753–1759.

Manuscript received Sept. 22, 2008, and revision received Jan. 5, 2009.